Pn tomography of the western United States using USArray

Janine S. Buehler[1] and Peter M. Shearer[1]

Received 10 August 2009; revised 21 May 2010; accepted 4 June 2010; published 30 September 2010.

[1] USArray has now provided several years of high-quality seismic data and improved ray coverage for much of the western United States, which will enable increased resolution for studies of the lithospheric and deeper structure of the North American continent. Here we analyze Pn arrival times from the transportable stations of USArray to resolve crustal thickness and uppermost mantle structure. We use 123,008 Pn picks from April 2004 to October 2009 as measured by the Array Network Facility at epicentral distances from 180 to 1450 km. These picks are derived from 778 stations at ~70 km spacing and 7903 earthquakes and quarry blasts. Applying the classic time-term method, we use a regularized least squares inversion to estimate crustal thickness variations and image velocity perturbations in the uppermost mantle just below the Moho. We also consider upper mantle anisotropy and describe the velocity perturbations with a cos 2ϕ azimuthal variation. Our crustal thickness map generally agrees with receiver function results from other researchers but differs in some details. We obtain an average upper mantle velocity of 7.93 km/s, with higher velocities beneath eastern Washington and northern Idaho, and lower velocities near the California-Mexico border, the Sierra Nevada, the northern coastal California region, and the greater Yellowstone area. We observe large anisotropic anomalies in southern California as well as in the Snake River Plain area. These results should complement other seismic studies (e.g., body and surface wave tomography and shear wave splitting) to provide information about composition, temperature, and tectonic processes in the western United States.

Citation: Buehler, J. S., and P. M. Shearer (2010), Pn tomography of the western United States using USArray, *J. Geophys. Res.*, *115*, B09315, doi:10.1029/2009JB006874.

1. Introduction

[2] Seismic tomography has the potential to provide detailed images of Earth structure, but is often limited by the coverage of the available seismic data. The USArray with its very dense and almost uniformly spaced stations has greatly improved tomographic resolution for much of the western United States. Prior to the installation of USArray in 2004, ray coverage was only dense in areas with regional seismic networks, as in California where many instruments are deployed along the San Andreas fault and various other seismogenic zones, whereas ray density was greatly reduced and nonuniform outside these areas. Many studies of Moho depth variations or upper mantle seismic velocities focused therefore on local areas with high station densities, as for example southern California [e.g., *Hearn*, 1984; *Zhu and Kanamori*, 2000].

[3] Pn tomography reveals information about the seismic velocities and anisotropy in the uppermost mantle as well as crustal thickness. Because of the large contrast in seismic velocities between the lower crust and the upper mantle and the shallow velocity gradient in the upper mantle, Pn tomographic velocity perturbation images show results for a very confined depth in the uppermost mantle, complementing surface wave or other body wave tomographies that average anomalies over larger depth intervals. Lateral variations in Pn velocities can be associated with temperature differences in the upper mantle, as well as compositional differences [e.g., *Goes and van der Lee*, 2002; *Perry et al.*, 2006].

[4] The crustal structure of the western United States is complex due to the very active tectonic regime. Crustal thickness and mantle anisotropy are fundamental in understanding tectonic history [*Savage and Silver*, 1993; *Silver*, 1996; *Zandt et al.*, 2004]. Therefore, isotropic as well as anisotropic velocity perturbations in the uppermost mantle below the western United States have been of interest and several Pn studies have been published [*Beghoul and Barazangi*, 1990; *Hearn et al.*, 1991; *Hearn*, 1996]. Alternative methods have also been applied to obtain information on crustal thickness and velocity structures in the upper mantle, which will provide points of comparison to our Pn results. Crustal thickness estimates have been obtained from surface waveform fitting [*Das and Nolet*, 1998], receiver function analysis [*Lewis et al.*, 2000; *Zhu and Kanamori*, 2000; *Yan and Clayton*, 2007; *Gashawbeza et al.*, 2008], and gravity data [*Mooney and Weaver*, 1989]. Anisotropy in

[1]Scripps Institution of Oceanography, University of California, San Diego, La Jolla, California, USA.

0148-0227/10/2009JB006874

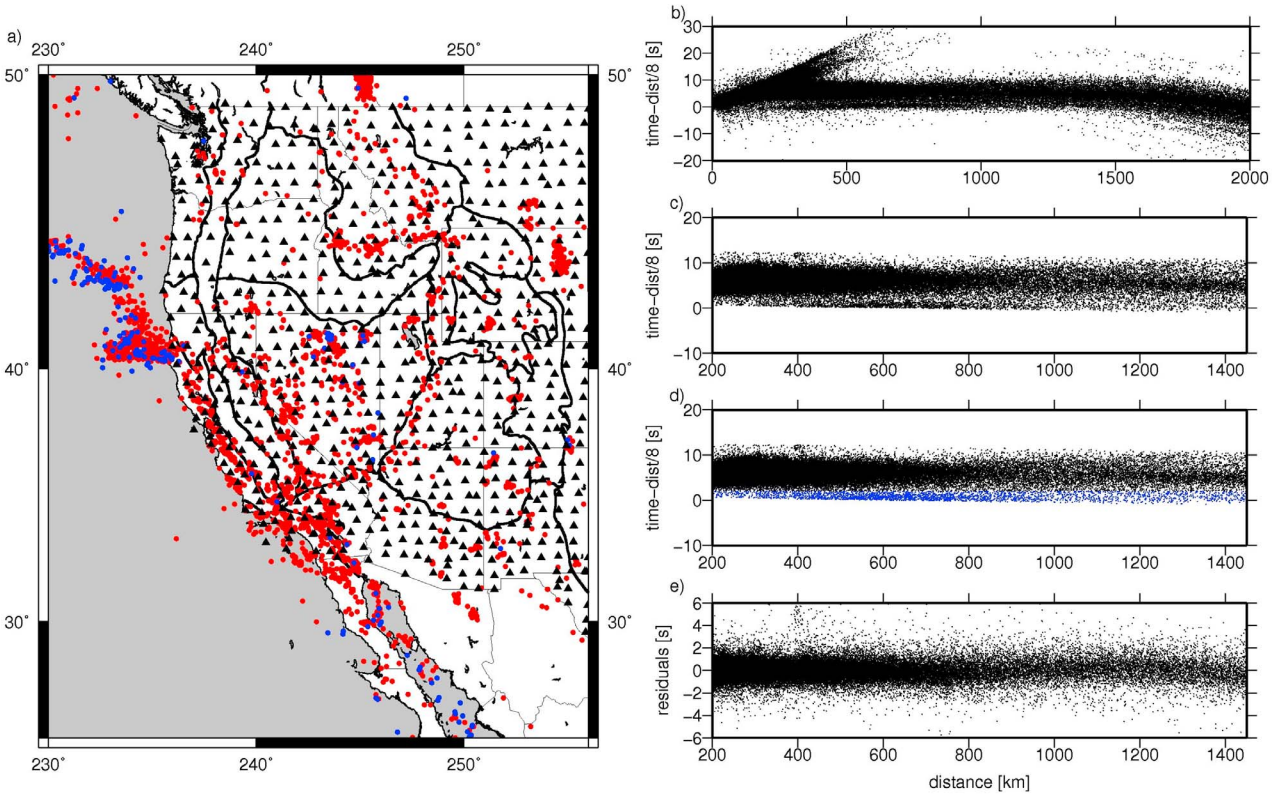

Figure 1. (a) Events (red circles) and USArray stations (black triangles) used in this study. (b) Time-distance plot of all available P wave picks with an epicentral distance smaller than 2000 km. (c) Picks left after the iterative windowing procedure. (d) Blue circles show early arrivals, mostly from offshore events (see Figure 1a). (e) Residuals after one-dimensional time term fit.

the upper mantle has mostly been studied with shear wave splitting [*Polet and Kanamori*, 2002; *Currie et al.*, 2004; *West et al.*, 2009]. In addition, improved seismic instrumentation has led to the development of new methods to extract information about the structure of the crust and uppermost mantle, for example using ambient noise tomography [*Yang et al.*, 2008; *Lin et al.*, 2009].

[5] This study is similar in approach to *Hearn* [1996], who performed anisotropic Pn tomography for the western United States, but benefits from a much more extensive data set. We determine both isotropic and anisotropic velocity perturbations in the uppermost mantle as well as crustal thickness using the densely spaced USArray stations. We start with several data processing steps to avoid using falsely identified Pn arrivals, and then use the Pn times to invert for velocity perturbations and crustal thickness. We also assess model resolution using various synthetic data sets. Finally, we discuss our results and compare them to other studies available in this area. Our results provide well-resolved Pn tomographic images that complement other seismic studies.

2. Data

[6] In this study we use first-arrival picks provided by the USArray Network Facility (ANF, http://anf.ucsd.edu/tools/events/download.php, last accessed October 2009). USArray consists of 400 transportable broadband seismometers, which are gradually crossing the United States, occupying sites for about 2 years on a 70 km grid. We use 778 station locations from −124.6°E to −100.1°E and from 29.5°N to 49.1°N, and events from −130°E to −100°E and from 25°N to 55°N (Figure 1a). In total we have 611,817 P wave arrivals (128,328 of which are labeled Pn) with epicentral distances smaller than 2000 km recorded between April 2004 and October 2009 (Figure 1b).

[7] In theory, Pn is the head wave that travels along the Moho within the uppermost mantle layer with an average velocity of about 8 km/s. However, in practice the complexity of the very heterogeneous crustal layer and the presence of velocity gradients beneath the Moho often make it difficult to distinguish the shallow turning P wave arrivals from the refracted Pn wave arrivals. Therefore, for certain picks the Pn label may not be correct, and we apply several processing steps to provide more reliable Pn picks. First we eliminate all the picks that are clearly not first arrivals. Next, we proceed in an iterative way similar to *Hearn et al.* [1991] and apply a number of constraints to the data: (1) epicentral distance between 180 km and 1450 km, (2) maximum hypocenter depth of 35 km, (3) maximum residual of 6 s after a straight line fit, (4) every event recorded by at least 5 stations, and (5) every station recorded Pn picks from at least 5 events. We limit the maximum distance to 1450 km since the residuals of the initial model form a straight line up to this distance on a residual-distance plot (Figure 1e), but start to curve at longer ranges. After the iterative windowing procedure, the final data set consists of 123,008 Pn picks

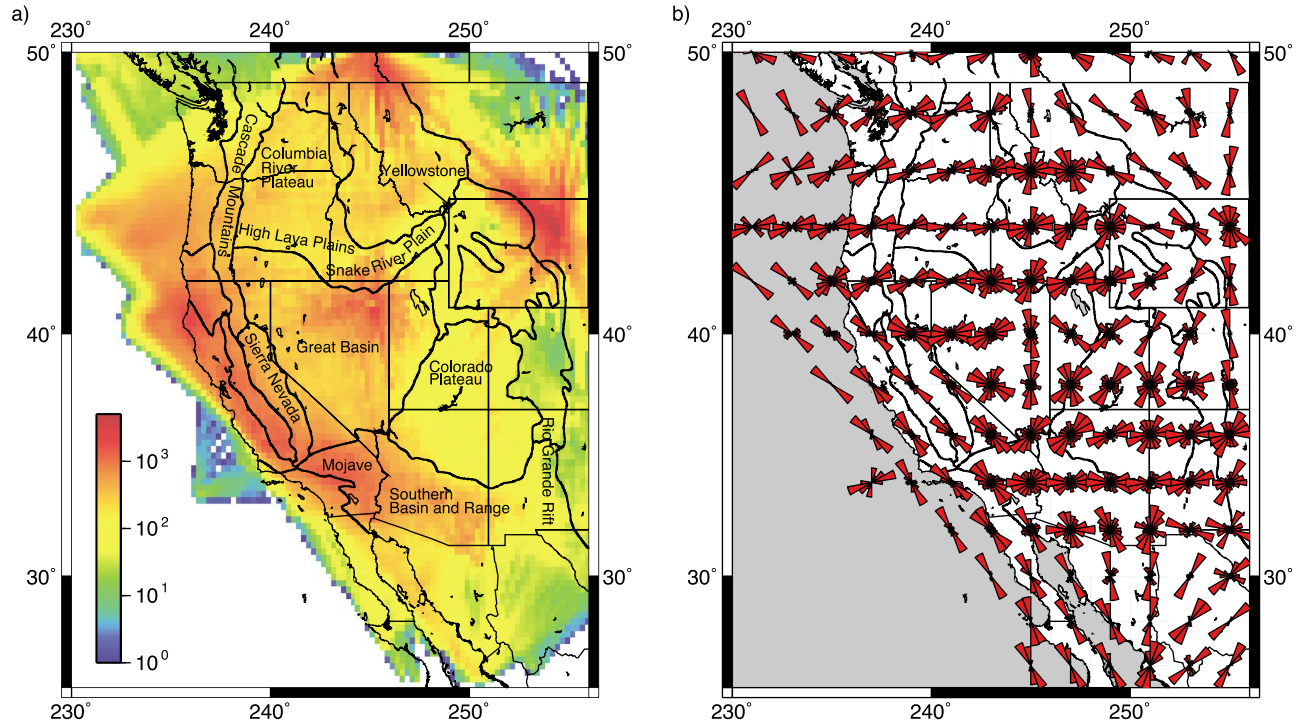

Figure 2. (a) Ray count per cell. (b) Azimuthal coverage, averaged over 64 cells (2° by 2°) in 20° bins in azimuth.

(65,299 with label Pn) from 7903 events (Figure 1c). The group of early arrivals seen in the plot results mainly from offshore events (Figures 1a and 1d) because of a thinner crust and/or higher velocities.

[8] Ray density is the highest in California because of its many seismically active areas. Lower ray coverage is observed in parts of the Basin and Range area and the Columbia River Plateau as well as east of −114°E (Figure 2a). Good azimuthal coverage for a large part of the western United States allows us to resolve azimuthal anisotropy (Figure 2b).

3. Method

3.1. One-Dimensional Modeling

[9] To obtain an initial estimate of the slowness in the uppermost mantle as well as crustal thickness variations, we set up a linear least squares problem following [*Hearn*, 1984]. If there is no significant vertical velocity gradient below the Moho, the Pn travel time can be described with three terms:

$$t_{es} = \tau_e + \tau_s + \Delta_{es} S, \quad (1)$$

where Δ_{es} is the great circle distance between the source and the receiver, S is the slowness in the uppermost mantle, and τ_e and τ_s are the event and station time terms, respectively. Crustal thicknesses are usually estimated from the station time terms only because of the relatively large uncertainties in hypocenter depth and earthquake origin time, which are absorbed into the event time terms [*Hearn*, 1984]. In the presence of a significant vertical velocity gradient in the uppermost mantle, additional terms would be needed to account for the fact that the arrivals are actually turning waves below the Moho [*Zhao*, 1993; *Phillips et al.*, 2007].

[10] The time term method of equation (1) achieves much better fits to our data than a simple straight line fit and can account for the travel time differences between the offshore and continental earthquakes. The straight line fit gives a mean velocity of 8.09 km/s and a large mean squared error of 2.5 s^2. By using equation (1), the event time term corrects for the thinner oceanic crust and the mean squared error is reduced to 0.42 s^2. A straight line fit to just the continental earthquakes reveals about the same mean velocity of 7.93 km/s as the one-dimensional time term estimation using all the earthquakes.

3.2. Two-Dimensional Modeling

[11] To include isotropic velocity perturbations as well as anisotropy, a two-dimensional grid is applied along the Moho and for each cell an isotropic as well as an anisotropic perturbation is taken into account [*Hearn*, 1996]. The Pn travel time residuals can then be described as

$$\delta t_{es} = \delta\tau_e + \delta\tau_s + \Sigma\Delta_{esk}(\delta S_k + A_k \cos 2\phi_{esk} + B_k \sin 2\phi_{esk}), \quad (2)$$

where Δ_{esk} is the distance the ray travels in the cell k, A_k and B_k are the anisotropic parameters for cell k, and ϕ is the back azimuth. We do not take the entire station-receiver distance into account, but only the distance the ray actually travels along the uppermost mantle. The horizontal offsets between the mantle piercing points and station locations are a function of Pn velocity, crustal velocity, and Moho depth, none of which are known a priori. The station and event time correction terms absorb errors in mantle pierce point location estimates as well as uncertainties in event location and

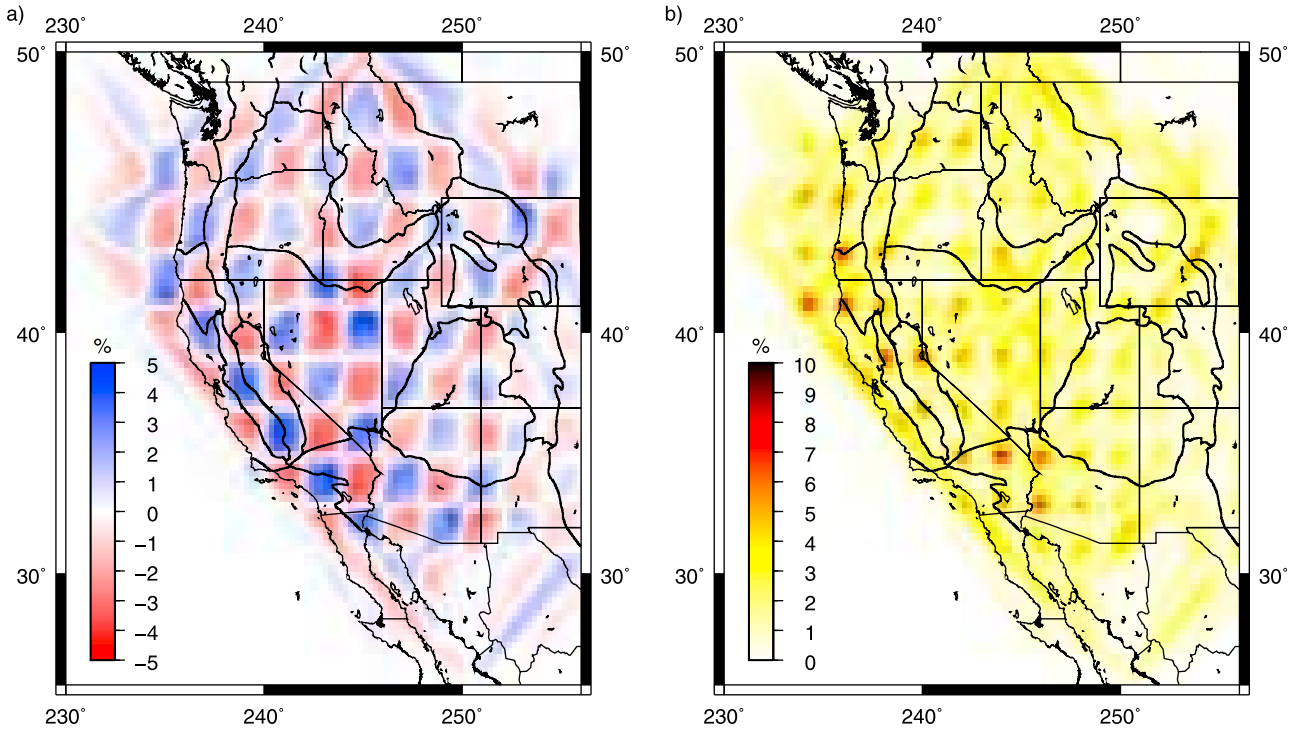

Figure 3. Checkerboard test: synthetic data are generated with ±5% isotropic perturbations only. (a) Recovered isotropic model. Red colors indicate recovered synthetic slow anomalies, and blue colors represent recovered fast anomalies. (b) Leakage into anisotropic model parameters.

origin time. Note that we neglect any possible 4ϕ azimuthal variations because previous studies of mantle anisotropy and models of aligned olivine crystals have generally found the 2ϕ terms to dominate [e.g., *Raitt et al.*, 1969; *Christensen*, 1984]. We solve the resulting problem $d = Gm$ in a least squares sense, where d is the data, m is the model, and G contains the kernels from equation (2). We simultaneously minimize the data misfit, model norm and model roughness:

$$\text{Minimize} \quad \| d - Gm \|^2 + \lambda_1 \| m \|^2 + \lambda_2 \| Lm \|^2, \qquad (3)$$

where L is the finite difference approximation of the Laplacian and λ_1 and λ_2 are the regularization parameters.

3.3. USArray Data Modeling Approach

[12] We start with the time term method and a uniform Pn velocity (equation (1)). This problem has 8682 model parameters and is small enough to permit a noniterative least squares inversion to solve for the slowness, station and event time terms. We apply no regularization to the time terms. Once we obtain a first-order estimate of the Moho topography and the mean upper mantle velocity, we estimate the location of the mantle pierce points, assuming the ray obeys Snell's law and a constant crustal velocity of 6.3 km/s. To image velocity perturbations and anisotropy, we then apply a regularized least squares inversion (equation (3)) using a conjugate gradient least squares approach [e.g., *Aster et al.*, 2005] to the travel time residuals (equation (2), with a cell size of 0.25° by 0.25°). We run these inversions for several different regularization parameters to obtain trade-off curves. We use separate parameters for the isotropic and the anisotropic regularization terms as well as for smoothing and damping (four regularization parameters in total). In practice, we seem to obtain the best results in terms of error and resolution trade-off for roughly equal damping and smoothing for the anisotropic and isotropic parameters. The station and event corrections are neither damped nor smoothed.

4. Results

4.1. Synthetic Data Resolution Tests

[13] To address the question of whether our ray coverage is sufficient for the methods applied, it would be ideal to apply a singular value decomposition and directly obtain resolution matrices [e.g., *Aster et al.*, 2005]. However, the large size of the problem makes it difficult to compute the generalized inverse. Therefore we use the classical checkerboard model approach to estimate the resolution and reliability of the inversion results.

[14] We calculate synthetic travel times using the same station event configuration as in the inversions with real data. We generate several synthetic data sets resulting from checkerboard perturbations with different sizes and amplitudes. The anomalies in Figure 3 are 2° by 2° (8 by 8 model cells) and have a mean slowness of 0.125 s/km. We compute synthetic travel times resulting from either isotropic or anisotropic velocity variations only, and also from combined isotropic and anisotropic perturbations. This procedure allows us to assess the resolution of the specific model parameters as well as the leakage of isotropic into anisotropic perturbations and vice versa [*Hearn*, 1996, 1999].

[15] Figure 3a shows the model obtained for synthetic travel times generated with isotropic perturbations only. The

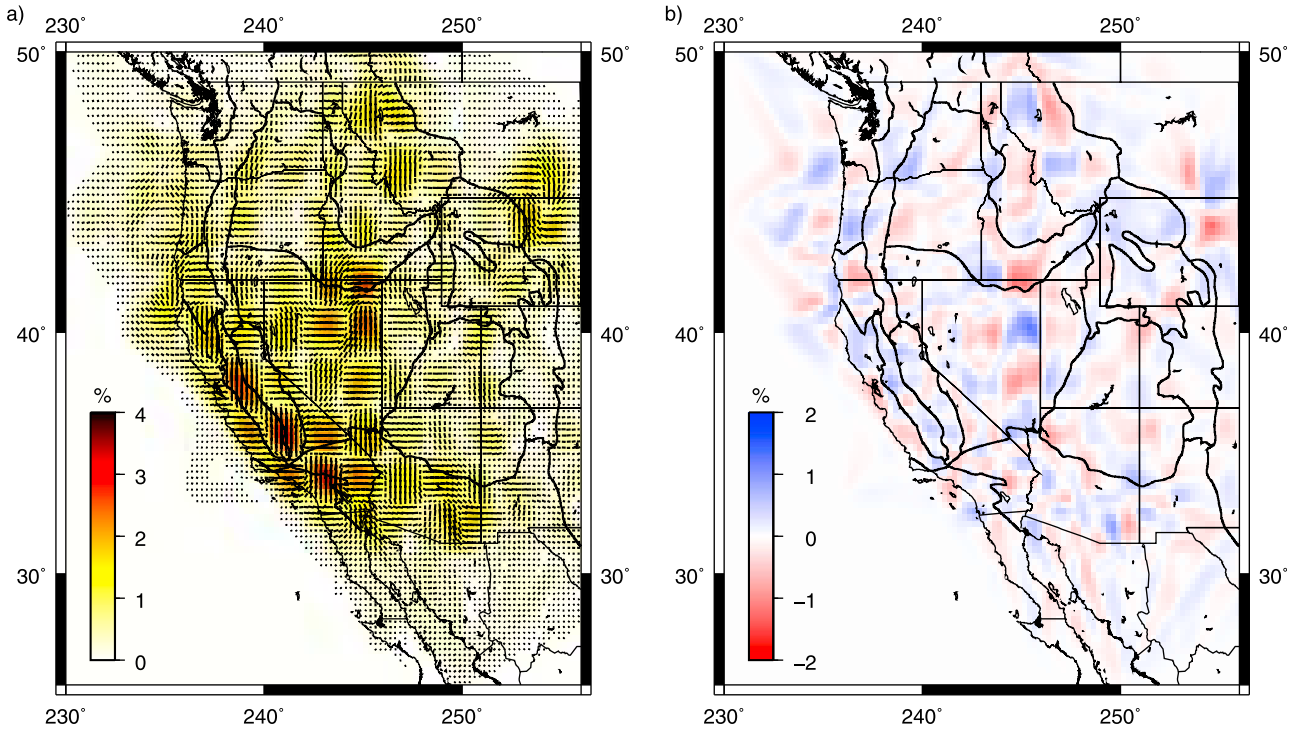

Figure 4. Checkerboard test: synthetic data are generated with 5% anisotropy only ($[V_{fast} - V_{slow}]/V_{iso} = 0.05$). (a) Recovered anisotropy model. (b) Leakage into isotropic model parameters.

perturbations vary ±5% in adjacent cells. Random noise with a standard deviation of 0.5 s is added. Figure 3b shows the leakage into anisotropic parameters, which is large at the corner of adjacent cells where the change in perturbations is the largest. This indicates that the anisotropic results may be less reliable in areas with sharp velocity contrasts. The amount of leakage depends on the choice of regularization parameters, here equal damping and smoothing is applied to all the parameters.

[16] Figure 4a shows the model obtained for synthetic travel times with anisotropic perturbations only. The data are generated assuming perpendicular fast directions in adjacent cells on a two degree grid. Generally, the fast axis is well resolved. The amplitude of the leakage into isotropic perturbations is small and shows a random pattern (Figure 4b).

[17] With the method described in section 3 (equations (1) and (2)), we obtain one delay time term per station. This term represents the average delay time over a cone defined by the ray incident angle and Moho depth. For this theory to be adequate, the Moho has to be fairly flat under a station. If the Moho topography has significant slopes, better accuracy would be obtained by allowing the station delay times to vary with azimuth. We tested the validity of the single time term assumption by generating a synthetic Moho topography and calculating synthetic travel times that consider the slopes in computing the mantle pierce points. To simplify the ray path calculations, we approximated the slope with a series of steps and assumed that the ray travels horizontally along the Moho in the vicinity of a station. The results show that crustal thicknesses can be resolved with reasonable accuracy using inversions that do not explicitly account for this effect. In addition, real data residual versus azimuth plots for USArray stations do not indicate significant slopes in the Moho topography. Finally, simple calculations of the effect of the inferred slopes reveal a negligible change in travel times if they are taken into account. Therefore the single station term method seems to be justified.

4.2. USArray Data

[18] Figure 5 shows the final model for the isotropic velocity perturbations resulting from the combined iso-anisotropic inversion (equation (2)). The mean squared residual resulting from this model is 0.34 s^2. The locations of the major anomalies correlate well with known active processes, as for example the large low-velocity anomalies in the Snake River Plain leading to the Yellowstone hot spot. Similar to *Hearn et al.* [1991], the main anomaly is not at the location of the Yellowstone caldera, but below the Snake River Plain. This could partly be because of the ray coverage gap at the current location of the caldera. In our image the lowest velocity occurs west of Hearn et al.'s main anomaly, in the area of the western Snake River Plain/Owyhee plateau. The amplitudes of the anomalies in the east might change with the advance of the transportable array since the synthetic test yields lower amplitudes close to the eastern model boundary where the data become more sparse.

[19] In agreement with *Hearn et al.* [1991] and *Hearn* [1996], a large low-velocity anomaly is also observed below the Sierra Nevada. The slow anomaly could either be caused by a mountain root or by warmer temperatures and partial melt beneath the mountain belt or a combination of both. The larger delay times in the Sierra seem to favor the mountain root theory. In southern California we obtain a large low-velocity zone west of the Salton Sea similar to

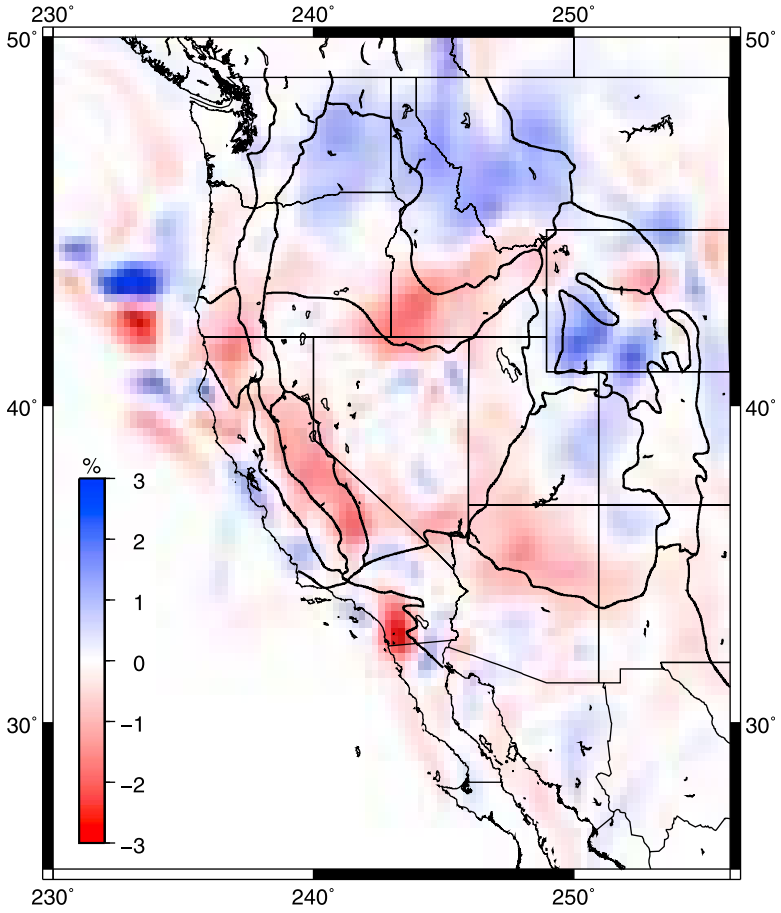

Figure 5. Isotropic velocity perturbations resulting from a simultaneous inversion for isotropic and anisotropic parameters. Red colors indicate areas of lower velocities, and blue colors indicate regions with higher velocities. The average velocity is 7.93 km/s.

Hearn [1984] and *Sung and Jackson* [1992], surrounded by less pronounced high-velocity perturbation areas.

[20] There is a significant high-velocity region in the north, spanning eastern Washington, northern Idaho and western Montana. This high-velocity zone is bounded to the south by the low-velocity region of the Snake River Plain but continues to the east with its highest velocities in southwestern Wyoming. High-resolution three-dimensional P wave tomography using USArray data shows that some of these fast anomalies can be observed to a depth of about 400 km [*Roth et al.*, 2008; *Burdick et al.*, 2008, 2009] and can be associated with the western edge of Precambrian North America.

[21] The velocity variations obtained from a purely isotropic model (no azimuth-dependent parameters included in the inversion) show similar patterns as the anomalies obtained from the combined inversion (Figure 6). The main difference is the higher amplitudes observed in Figure 6; however, the locations of the anomalies are stable. The mean squared residual of this model is 0.36 s^2.

[22] The Pn anisotropic modeling results generally show a quite complex image. We obtain large anisotropic anomalies in the Great Basin desert, off the coast of northern California as well as in southern California/northern Mexico (Figure 7). In central California, the fast axis is mostly fault-parallel, indicating that the anisotropy is caused by shearing along the plate boundary. Similar to the work by *Hearn* [1996] we find that the fast axis is not parallel to the plate boundary in all of southern California, but that the fast direction orients east–west, especially in the Mojave Desert. *Hearn* [1996] discusses the possibility of the north–south compression in southern California as the cause of the perpendicular east–west anisotropic direction.

[23] We find a fairly homogeneous northeast fast axis in the northwestern Basin and Range, which then turns into a rotational feature in eastern Nevada. In the southern Basin and Range the fast direction orients southeast–northwest. Off coastal Oregon there is strong east–west anisotropy, which could be correlated with the subduction zone. However, large isotropic anomalies can also be observed in this area, which could indicate a modeling artifact since azimuthal coverage in these cells is limited.

[24] The station terms account for the time it takes the ray to travel from the mantle pierce point to the receiver. Positive station time terms indicate a thicker crust, however there is a tradeoff between contributions from low-velocity anomalies in the crust and deeper Moho depths. Nevertheless, the larger the delay is, the more likely it has some significant contributions from Moho depth deviations. We use an average crustal velocity of 6.3 km/s to estimate absolute Moho depths. Several large delays can be observed, i.e., in areas where a compensating root is expected, as in the Sierra

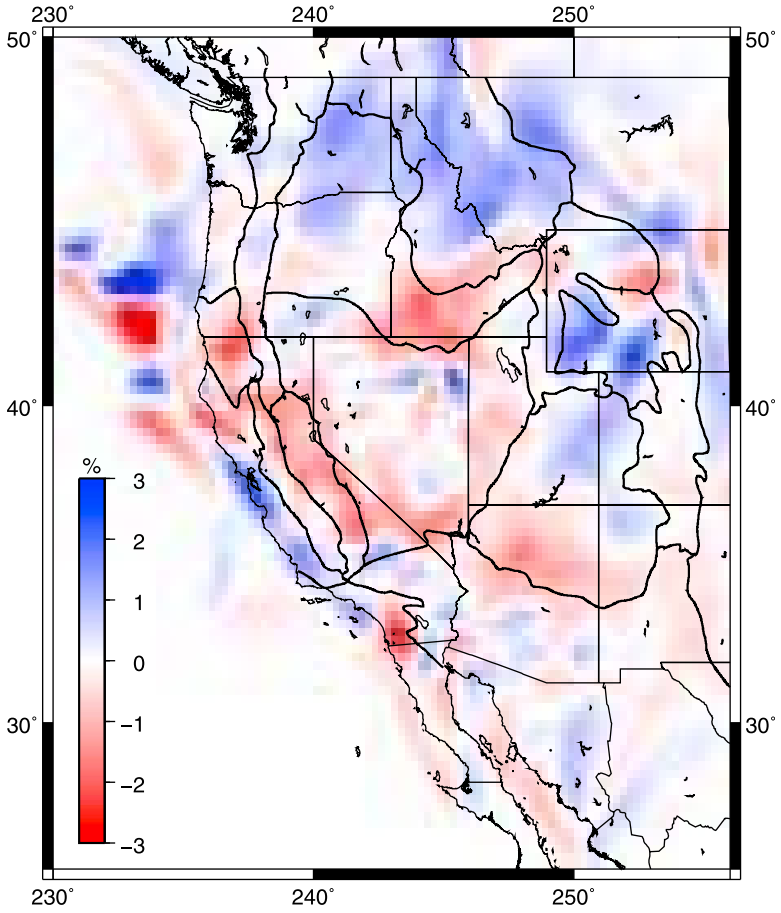

Figure 6. The velocity variations obtained from an isotropic model only (no azimuth-dependent parameters included in the inversion).

Nevada as well as the Cascade Range (Figure 8). This is in agreement with the slow velocity anomalies observed below this entire mountain chain (Figure 5). The thickest crust is imaged in southern Wyoming, however in this part of the model the resolution is reduced.

[25] In the northern Basin and Range province (Nevada and part of Utah) crustal thickness is reduced as expected in an extensional tectonic regime. The crust is also thinner below the coastal ranges of California and below much of southern California. The thinner crust in the southern Basin and Range is very distinct, with thicker crust indicated to the north below the Colorado Plateau. Similar crustal thicknesses can be observed from surface waveform fitting [*Das and Nolet*, 1998].

[26] In addition to Pn studies, receiver function analyses are widely used to estimate crustal thickness. With receiver functions a crustal thickness estimate is obtained below every station considered, due to P to S wave conversions at the crust-mantle boundary. Many such studies exist, especially for the area of the Basin and Range and southern California [*Lewis et al.*, 2000; *Zhu and Kanamori*, 2000; *Yan and Clayton*, 2007]. *Gilbert and Sheehan* [2004] estimate crustal thickness across the Great Basin, Colorado Plateau, Rocky Mountain, and the great Plains Provinces. Similar to our results, *Gilbert and Sheehan* [2004] find that the crust thins in the Basin and Range. Their thinnest crust is confined to northern Nevada and northern Utah, but we also find crust with similar thinness in central western Utah. Both the results of *Gilbert and Sheehan* [2004] and our station term results indicate thicker crust below the Rocky Mountains. However, they have their thickest crust in northwestern Colorado whereas our Pn study images its thickest crust in southern Wyoming.

[27] Receiver functions from USArray (A. Levander, personal communication, 2009) agree with our station delays at large scale. The receiver function results show a somewhat greater average Moho depth of 38 km in the western United States compared to the average crustal thickness determined by the station terms (34 km). This discrepancy is likely caused by differences in the assumed crustal velocity structure used in each method to compute the Moho depths. With the time term method we solve for relative station terms, measure the intersect time of a straight line fit to data from continental earthquakes, and compute the mean Moho depth assuming an average crustal P wave velocity of 6.3 km/s. However, using a crustal velocity of 6.58 km/s would increase our mean Moho depth estimate to 38 km, in agreement with the receiver function analysis. Further analysis will be required to determine which absolute Moho depth estimate is more accurate. Here we focus simply on comparing relative Moho depths. Using the Pn depths obtained using the higher crustal velocity, 65% of the receiver function thickness estimates are within ±5 km of the Pn results and only 12% of the results have a larger dif-

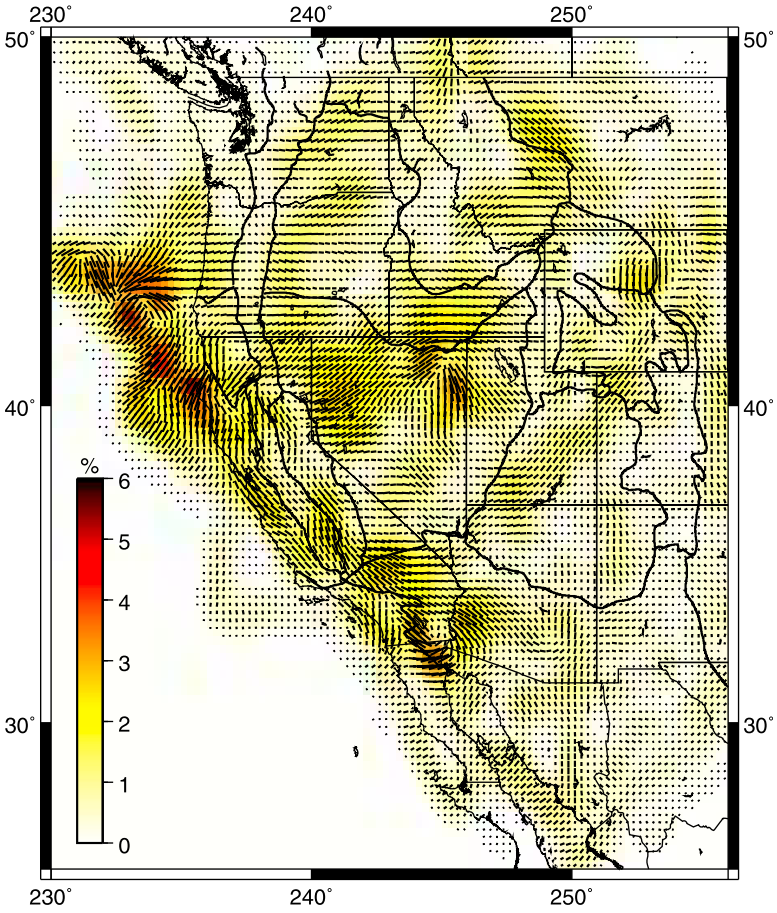

Figure 7. The azimuthal anisotropy model. The black lines indicate the Pn fast axis with the length of the line proportional to the strength of the anisotropy. The anisotropy strength is also colored by percent (see scale).

ference than 10 km. Consistent with the Pn results, the USArray receiver function analyses show that the southern Basin and Range province has relatively thin crust versus thicker crust observed beneath the southwestern Colorado Plateau. In addition, the Pn and receiver function results both show thicker crust in the Sierra Nevada as well as the Cascade Range, and a thin crust in the eastern Great Basin. The main differences are that receiver functions show thinner crust in a wider band along most of the west coast and up to ~20 km thicker crust in eastern Montana. The estimates in the east will likely become more accurate for USArray studies with the advance of the temporary stations.

5. Discussion and Conclusions

[28] Many mantle velocity and crustal thickness studies in the western United States provide an opportunity to compare results. Because Pn is sensitive to only a small depth interval at the very top of the mantle, it provides an important constraint on other methods, which vertically average features in the upper mantle. With USArray, we expect to obtain more detailed Pn velocity maps than previous studies. Applying the data selection process described by *Hearn* [1996] to our data set, USArray still provides more than twice the number of picks for the same area as previous studies, with improved ray coverage at varying angles, which is important to produce accurate azimuthal anisotropy maps.

[29] Azimuthal anisotropy in the upper mantle can be estimated using several different data sets, such as surface waves and Pn and SKS arrivals. With shear wave splitting measurements, usually from the SKS phase, anisotropy below individual stations can be determined. Both shear wave splitting and surface wave results provide a vertically integrated measure of anisotropy in the upper mantle whereas the Pn results constrain the anisotropy in the uppermost mantle lid. Differences in anisotropy between shear wave splitting and Pn studies can therefore indicate vertical changes in anisotropy.

[30] The most pronounced feature of recent USArray shear wave splitting studies is the small splitting times in the central Great Basin, surrounded by fast polarization directions in a cylindrical pattern [*Liu*, 2009; *West et al.*, 2009] (Figure 9). In addition, new high-resolution P wave tomographic models using USArray of the same area reveal a near vertical cylindrical zone of increased P wave velocities [*Roth et al.*, 2008; *West et al.*, 2009], ranging from a depth of about 75 km to at least 500 km. *Burdick et al.* [2008, 2009] use USArray P wave arrivals combined with P wave travel times from other sources, such as reprocessed ISC data, to constrain 3-D heterogeneity in the upper mantle beneath North America. *Burdick et al.* [2009] also observe a

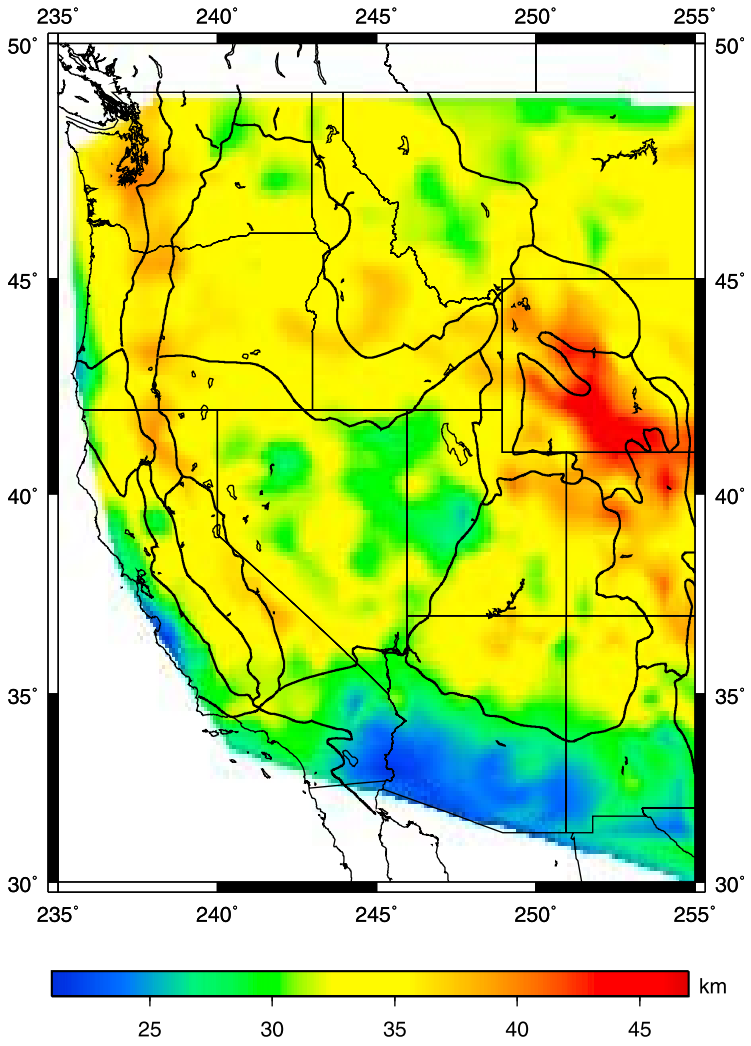

Figure 8. Crustal thickness estimates from station time terms. Crustal velocity is assumed to be constant at 6.3 km/s.

deep fast anomaly below central Nevada, but which only appears below about 200 km. The location of this high-velocity anomaly coincides with the region of smallest splitting times. *West et al.* [2009] suggest that a lithospheric drip beneath the central Great Basin causes these seismic observations, i.e., that the downward flow generates a shift from azimuthal to radial anisotropy. This circular pattern of fast polarization directions centered in the eastern Great Basin has been noted before at lower resolution and alternate models were proposed to explain this feature; *Savage and Sheehan*'s [2000] preferred model consists of vertically upwelling asthenospheric material beneath the northern Great Basin in combination with lateral asthenospheric flow because of lithospheric drag parallel to the absolute plate motion. *Zandt and Humphreys* [2008] propose that a simple rollback of a narrow slab can predict this circular SKS pattern and argue that there is no evidence for an active plume beneath central Nevada; they suggest that the combination of westward slab rollback of the Gorda-Juan de Fuca slab and northward opening of the slab window promotes a strong toroidal mantle flow.

[31] The Pn tomography plot (Figure 7) also shows an area of almost no anisotropy in central Nevada, however of much less spacial extent than in the shear wave splitting. Pn results also suggest that the fast axis rotates around the anisotropy low, however this pattern is less smooth and distinct compared to the fast polarization direction of the vertically traveling shear waves. In contrast to the P wave tomography [*West et al.*, 2009], Pn isotropic velocity anomalies indicate no significant fast structures in the central Great Basin (Figure 5). The imaged Pn anisotropy variations by *Hearn* [1996] show a similar low in the central Great Basin, but with strong northwest oriented anisotropy in the southeast.

[32] *Lin et al.* [2009] apply a new surface wave tomographic method based on tracking wave fronts across the USArray using ambient noise recordings. Their 24 s period Rayleigh wave azimuthal anisotropy maps reveal similar fast directions as the Pn model. The extent of the low-anisotropy area is also much smaller in the central Great Basin than for the shear wave splitting results, and, similar to our model, stronger northeast–southwest anisotropy can be observed in northwestern Nevada. All three methods

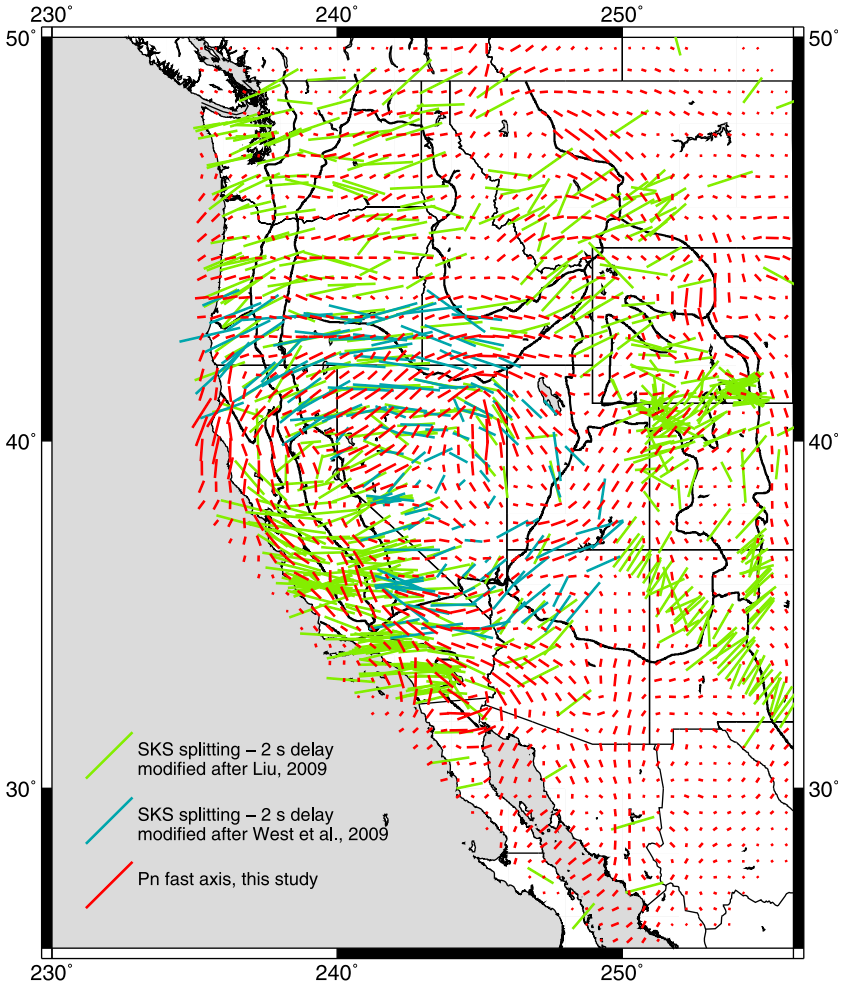

Figure 9. Comparison of shear wave splitting fast polarization directions (blue and green colors) and the Pn fast axis (red) in the western United States. The shear wave splitting results are modified after *Liu* [2009] and *West et al.* [2009].

agree on east–west fast directions north of the Great Basin. Similar to the Pn velocity perturbations, the 24 s Rayleigh isotropic phase speed shows a more diffuse low-velocity anomaly in the central Great Basin. The surface wave and Pn anisotropy models are in better general agreement with each other than they are with the splitting results, which include sensitivity to anisotropy deeper in the mantle. These different results indicate that there is not a consistent vertically coherent mechanism that generates anisotropy throughout the upper mantle. The less pronounced features of the Pn study suggest that the shear wave splitting observations result mostly from sublithospheric mantle flow although anisotropy in the lithosphere might contribute to the circular pattern.

[33] North of the Great Basin and in the back arc of the Juan the Fuca subduction zone are the Columbia River Basalts, the High Lava Plains in Oregon, and the Yellowstone-Snake River Plain volcanic system. The eastern Snake River Plain is topographically depressed and its volcanism tracks approximately parallel to the motion of the North American plate. The Plain exhibits age progression in volcanism originating from northern Nevada and extending toward the current location of the Yellowstone caldera [*Christiansen et al.*, 2002].

[34] Studies of shear wave splitting in the eastern Snake River Plain [e.g., *Schutt et al.*, 1998; *Waite et al.*, 2005] imply a relatively simple anisotropic structure. The fast directions (~N60°E) are roughly parallel to the absolute plate motion and can be explained with asthenospheric flow. However, the fast directions rotate from ~N60°E to ~N100°E in the central Snake River Plain and then back to N70°E in the western Snake River Plain [*Walker et al.*, 2004]. These variations cannot be explained with a simple asthenospheric flow model; instead they can be recognized as part of the rotation around the Great Basin. Following *Savage and Sheehan* [2000], *Walker et al.* [2004] propose a similar parabolic flow model which expands upon the simpler model by adding an upwelling effect in central Nevada.

[35] Similar to the splitting results, the Pn fast axes from this study rotate from SW–NE in the western Snake River Plain to ESE–WNW directions in the central Snake River Plain. However the Pn fast axes do not rotate back in the eastern Snake River Plain except in the most northeastern part, but keep the same ESE–WNW to E–W orientation. A

lower-resolution Pn study by *Smith and Ekstrom* [1999] confirms mostly E–W orientation fast axes beneath the eastern Snake River Plain. This supports the assumption that the SKS fast polarization directions in the eastern Snake River Plain are caused by plate motion parallel asthenospheric flow and that the strain field in the uppermost mantle is dominated by local processes.

[36] In addition to the varying angles, the delay times on the eastern Snake River Plain are significantly smaller (~1 s) than along its flanks (~1.8 s) which is not predicted by either of the flow models. To explain these shorter delay times, Walker et al. [2004] present three hypothesis, one of them being lower crustal flow away from the eastern Snake River Plain, which would suggest a lattice preferred orientation of olivine in the uppermost mantle with a NNW–SSE fast direction below the plain. This hypothesis is not supported by the Pn anisotropy results, as the fast axes are primarily east–west oriented. Alternate explanations include the presence of magma-filled lenses in the lithosphere and compositional segregation.

[37] Adjacent to the volcano track of the Snake River Plain, and originating at the same time at the Owyhee Plateau ~15 Ma years ago, is the volcanism of the High Lava Plains [*Christiansen et al.*, 2002]. Although the common place of origin seems to suggest a common source, the volcano track of the Snake River Plain is roughly parallel to the motion of the North American plate whereas the High Lava Plain volcanic track heads almost in a perpendicular direction. Our Pn fast axes are not parallel to the volcanic High Lava Plain track, but rotate from SW–NE fast directions in southern Oregon to E–W fast axes in central Oregon before they rotate back to a more plate-motion-parallel direction.

[38] A recent shear wave splitting study of the High Lava Plain region by *Long et al.* [2009] that uses data recorded by USArray stations as well as temporary experiments shows fast polarization directions of the SKS phase that are nearly uniform E-W aligned. Contrary to these shear wave splitting results, which show larger splitting delay times in the High Lava Plains (>1.5 s) than in the eastern Snake River Plain (~1–1.5 s), we observe much less Pn anisotropy in southeastern Oregon (~0.5%) than in southern Idaho (~2.5%). Synthetic tests show that the amplitude of Pn anisotropy is generally not well resolved north of 42°N. However since the magnitude and fast directions of the Pn and SKS anisotropy differ in eastern Oregon, it is probable that the largest contributions to the observed splitting parameters originate below the uppermost mantle lid and are most likely associated with mantle flow. This is consistent with the unusually large delay times that are observed in the High Lava Plains, which are more reasonable to explain with asthenospheric flow than with a very large magnitude of anisotropy in the lithosphere [*Long et al.*, 2009].

[39] Ray coverage is reduced beneath the southern Rocky Mountains and the Colorado Plateau and we will be able to make more accurate comparisons once USArray moves further east. At current resolution, we obtain a significant low-velocity anomaly beneath Arizona, which includes the region beneath the southwestern Colorado Plateau. Recent USArray P wave tomography results show a similar slow anomaly at 100 km depth [*Burdick et al.*, 2009]. Similar to a local Pn study [*Lastowka and Sheehan*, 2005], we also find reduced velocities beneath the Rio Grande Rift. SKS splitting results across the Rio Grande Rift and the Colorado Plateau show fast directions that are generally uniform and subparallel to the North American plate motion [e.g., *Gok et al.*, 2003]. In contrast, the Pn fast axes show a complex picture for most of the southern Rocky Mountain region but are not yet completely reliable.

[40] The complex tectonic setting in California is shown in many seismic anisotropy studies that investigate upper mantle dynamics [*Hearn*, 1984; *Sung and Jackson*, 1992; *Polet and Kanamori*, 2002; *Davis*, 2003]. In California, we observe mostly San Andreas fault parallel anisotropy, which turns into a more east–west orientation in the Mojave Desert and northern Mexico. The orientations of the fast axes are generally similar to the ones previously obtained by *Hearn* [1996] and correspond with the surface wave tomography results at large scale [*Lin et al.*, 2009].

[41] *Polet and Kanamori* [2002] determine anisotropy beneath California from shear wave splitting measurements. Similar to our Pn anisotropy results (Figure 7), they find northeast oriented fast directions in northern California, a more NW–SE fast direction in central California, and E–W anisotropy in the Mojave. *Polet and Kanamori* [2002] find variations in splitting parameters with polarization azimuth for stations in the greater San Francisco Bay Area and are able to model these observations with a two-layer anisotropy model, in which a thin layer with a fast direction parallel to the San Andreas fault is above a layer with an E–W fast polarization direction. In apparent agreement with this two-layer model, the Pn fast axes in central California are mainly fault parallel aligned whereas the fast SKS polarization directions are rotated toward an E–W direction.

[42] In Oregon, our Pn results indicate mostly east–west fast directions, which then rotate to a more NE–SW orientation in Washington. Generally the Pn anisotropy is less reliable for the area north of the Great Basin, since the azimuthal coverage is worse. Except for the large anisotropic perturbations off the coast of Oregon, the Pn results suggest very little anisotropy in the fore arc of the Cascadia subduction zone. We consider the large perturbations off the coast of northern California and Oregon likely to be an inversion artifact because of reduced azimuthal ray coverage in this area. In contrast, shear wave splitting suggests fast directions parallel to the subduction direction of the Juan de Fuca plate for a large part of the fore arc of the Cascadia subduction zone with delay times larger than 1 s [*Currie et al.*, 2004]. In the back arc, the Pn as well as the shear wave anisotropy show similar fast directions parallel to the convergence of the Pacific and North American plates.

[43] Although anisotropy cannot be resolved equally well in the northwestern United States, USArray provides a greatly improved data set with good station and event coverage. Synthetic tests show that anomalies as small as 1° by 1° can be resolved for much of the western United States. Currently California and the Basin and Range areas are best resolved, however, as the transportable array moves east, resolution will improve east of the Great Basin. The Pn inversion results show prominent features of crustal thickness and velocity perturbations, many of which are observed throughout the region from studies using different data sets. The Pn anisotropy results are complementary to shear wave splitting, suggesting in several regions that the orientation of azimuthal anisotropy changes with depth in the uppermost mantle.

[44] **Acknowledgments.** We thank Luciana Astiz and the operators of the Array Network Facility for making their phase picks available and Thomas Hearn and an anonymous reviewer for their constructive comments. This research was funded by grant EAR-0710881 from the National Science Foundation.

References

Aster, R., B. Borchers, and C. Thurber (2005), *Parameter Estimation and Inverse Problems*, Elsevier, New York.

Beghoul, N., and M. Barazangi (1990), Azimuthal anisotropy of velocity in the mantle lid beneath the Basin and Range province, *Nature*, *348*(6301), 536–538, doi:10.1038/348536a0.

Burdick, S., et al. (2008), Upper mantle heterogeneity beneath North America from travel time tomography with global and USArray transportable array data, *Seismol. Res. Lett.*, *79*(3), 384–392, doi:10.1785/gssrl.79.3.384.

Burdick, S., R. D. van der Hilst, F. L. Vernon, V. Martynov, T. Cox, J. Eakins, T. Mulder, L. Astiz, and G. L. Pavlis (2009), Model update December 2008: Upper mantle heterogeneity beneath North America from P-wave travel time tomography with global and USArray transportable array data, *Seismol. Res. Lett.*, *80*(4), 638–645, doi:10.1785/gssrl.80.4.638.

Christensen, N. I. (1984), The magnitude, symmetry and origin of upper mantle anisotropy based on fabric analyses of ultramafic tectonites, *Geophys. J. R. Astron. Soc.*, *76*(1), 89–111.

Christiansen, R. L., G. R. Foulger, and J. R. Evans (2002), Upper-mantle origin of the Yellowstone hotspot, *Geol. Soc. Am. Bull.*, *114*(10), 1245–1256, doi:10.1130/0016-7606(2002)114<1245:UMOOTY>2.0.CO;2.

Currie, C. A., J. F. Cassidy, R. D. Hyndman, and M. G. Bostock (2004), Shear wave anisotropy beneath the Cascadia subduction zone and western North American craton, *Geophys. J. Int.*, *157*(1), 341–353, doi:10.1111/j.1365-246X.2004.02175.x.

Das, T., and G. Nolet (1998), Crustal thickness map of the western United States by partitioned waveform inversion, *J. Geophys. Res.*, *103*(B12), 30,021–30,038, doi:10.1029/98JB01119.

Davis, P. M. (2003), Azimuthal variation in seismic anisotropy of the southern California uppermost mantle, *J. Geophys. Res.*, *108*(B1), 2052, doi:10.1029/2001JB000637.

Gashawbeza, E. M., S. L. Klemperer, C. K. Wilson, and E. L. Miller (2008), Nature of the crust beneath northwest Basin and Range province from teleseismic receiver function data, *J. Geophys. Res.*, *113*, B10308, doi:10.1029/2007JB005306.

Gilbert, H. J., and A. F. Sheehan (2004), Images of crustal variations in the intermountain west, *J. Geophys. Res.*, *109*, B03306, doi:10.1029/2003JB002730.

Goes, S., and S. van der Lee (2002), Thermal structure of the North American uppermost mantle inferred from seismic tomography, *J. Geophys. Res.*, *107*(B3), 2050, doi:10.1029/2000JB000049.

Gök, R., et al. (2003), Shear wave splitting and mantle flow beneath LA RISTRA, *Geophys. Res. Lett.*, *30*(12), 1614, doi:10.1029/2002GL016616.

Hearn, T. M. (1984), Pn travel times in southern California, *J. Geophys. Res.*, *89*(B3), 1843–1855, doi:10.1029/JB089iB03p01843.

Hearn, T. M. (1996), Anisotropic Pn tomography in the western United States, *J. Geophys. Res.*, *101*(B4), 8403–8414, doi:10.1029/96JB00114.

Hearn, T. M. (1999), Uppermost mantle velocities and anisotropy beneath Europe, *J. Geophys. Res.*, *104*(B7), 15,123–15,139, doi:10.1029/1998JB900088.

Hearn, T., N. Beghoul, and M. Barazangi (1991), Tomography of the western United-States from regional arrival times, *J. Geophys. Res.*, *96*(B10), 16,369–16,381, doi:10.1029/91JB01509.

Lastowka, L. A., and A. F. Sheehan (2005), CDROM interstation Pn study along the Rio Grande Rift, in *The Rocky Mountain Region: An Evolving Lithosphere: Tectonics, Geochemistry, and Geophysics*, *Geophys. Monogr. Ser.*, vol. 154, edited by K. E. Karlstrom and G. R. Keller, pp. 379–384, AGU, Washington, D. C.

Lewis, J. L., S. M. Day, H. Magistrale, J. Eakins, and F. Vernon (2000), Regional crustal thickness variations of the Peninsular Ranges, southern California, *Geology*, *28*(4), 303–306, doi:10.1130/0091-7613(2000)28<303:RCTVOT>2.0.CO;2.

Lin, F. C., M. H. Ritzwoller, and R. Snieder (2009), Eikonal tomography: Surface wave tomography by phase front tracking across a regional broad-band seismic array, *Geophys. J. Int.*, *177*(3), 1091–1110, doi:10.1111/j.1365-246X.2009.04105.x.

Liu, K. H. (2009), NA-SWS-1.1: A uniform database of teleseismic shear wave splitting measurements for North America, *Geochem. Geophys. Geosyst.*, *10*, Q05011, doi:10.1029/2009GC002440.

Long, M. D., H. Gao, A. Klaus, L. S. Wagner, M. J. Fouch, D. E. James, and E. D. Humphreys (2009), Shear wave splitting and the pattern of mantle flow beneath eastern Oregon, *Earth Planet. Sci. Lett.*, *288*, 359–369, doi:10.1016/j.epsl.2009.09.039.

Mooney, W. D., and C. S. Weaver (1989), Regional crustal structure and tectonics of the Pacific coastal states: California, Oregon, and Washington, in *Geophysical Framework of the United States*, edited by L. A. Pakiser and W. D. Mooney, *Geol. Soc. Am. Mem.*, 172, 129–162.

Perry, H. K. C., C. Jaupart, J. -C. Mareschal, and N. M. Shapiro (2006), Upper mantle velocity-temperature conversion and composition determined from seismic refraction and heat flow, *J. Geophys. Res.*, *111*, B07301, doi:10.1029/2005JB003921.

Phillips, W. S., M. L. Begnaud, C. A. Rowe, L. K. Steck, S. C. Myers, M. E. Pasyanos, and S. Ballard (2007), Accounting for lateral variations of the upper mantle gradient in Pn tomography studies, *Geophys. Res. Lett.*, *34*, L14312, doi:10.1029/2007GL029338.

Polet, J., and H. Kanamori (2002), Anisotropy beneath California: Shear wave splitting measurements using a dense broadband array, *Geophys. J. Int.*, *149*(2), 313–327, doi:10.1046/j.1365-246X.2002.01630.x.

Raitt, R. W., G. G. Shor, T. J. G. Francis, and G. B. Morris (1969), Anisotropy of Pacific upper mantle, *J. Geophys. Res.*, *74*(12), 3095–3109, doi:10.1029/JB074i012p03095.

Roth, J. B., M. J. Fouch, D. E. James, and R. W. Carlson (2008), Three-dimensional seismic velocity structure of the northwestern United States, *Geophys. Res. Lett.*, *35*, L15304, doi:10.1029/2008GL034669.

Savage, M. K., and A. F. Sheehan (2000), Seismic anisotropy and mantle flow from the Great Basin to the Great Plains, western United States, *J. Geophys. Res.*, *105*(B6), 13,715–13,734, doi:10.1029/2000JB900021.

Savage, M. K., and P. G. Silver (1993), Mantle deformation and tectonics: Constraints from seismic anisotropy in the western United States, *Phys. Earth Planet. Inter.*, *78*(3–4), 207–227, doi:10.1016/0031-9201(93)90156-4.

Schutt, D., E. D. Humphreys, and K. Dueker (1998), Anisotropy of the Yellowstone hot spot wake, eastern Snake River Plain, Idaho, *Pure Appl. Geophys.*, *151*(2–4), 443–462, doi:10.1007/s000240050122.

Silver, P. G. (1996), Seismic anisotropy beneath the continents: Probing the depths of geology, *Annu. Rev. Earth Planet. Sci.*, *24*, 385–432, doi:10.1146/annurev.earth.24.1.385.

Smith, G. P., and G. Ekstrom (1999), A global study of Pn anisotropy beneath continents, *J. Geophys. Res.*, *104*(B1), 963–980, doi:10.1029/1998JB900021.

Sung, L. Y., and D. D. Jackson (1992), Crustal and uppermost mantle structure under southern California, *Bull. Seismol. Soc. Am.*, *82*(2), 934–961.

Waite, G. P., D. L. Schutt, and R. B. Smith (2005), Models of lithosphere and asthenosphere anisotropic structure of the Yellowstone hot spot from shear wave splitting, *J. Geophys. Res.*, *110*, B11304, doi:10.1029/2004JB003501.

Walker, K. T., G. H. R. Bokelmann, and S. L. Klemperer (2004), Shear-wave splitting beneath the Snake River Plain suggests a mantle upwelling beneath eastern Nevada, USA, *Earth Planet. Sci. Lett.*, *222*(2), 529–542, doi:10.1016/j.epsl.2004.03.024.

West, J. D., M. J. Fouch, J. B. Roth, and L. T. Elkins-Tanton (2009), Vertical mantle flow associated with a lithospheric drip beneath the Great Basin, *Nat. Geosci.*, *2*(6), 439–444, doi:10.1038/ngeo526.

Yan, Z. M., and R. W. Clayton (2007), Regional mapping of the crustal structure in southern California from receiver functions, *J. Geophys. Res.*, *112*, B05311, doi:10.1029/2006JB004622.

Yang, Y., M. H. Ritzwoller, F. -C. Lin, M. P. Moschetti, and N. M. Shapiro (2008), Structure of the crust and uppermost mantle beneath the western United States revealed by ambient noise and earthquake tomography, *J. Geophys. Res.*, *113*, B12310, doi:10.1029/2008JB005833.

Zandt, G., and E. Humphreys (2008), Toroidal mantle flow through the western US slab window, *Geology*, *36*(4), 295–298, doi:10.1130/G24611A.1.

Zandt, G., H. Gilbert, T. J. Owens, M. Ducea, J. Saleeby, and C. H. Jones (2004), Active foundering of a continental arc root beneath the southern Sierra Nevada in California, *Nature*, *431*(7004), 41–46, doi:10.1038/nature02847.

Zhao, L. S. (1993), Lateral variations and azimuthal isotropy of Pn velocities beneath Basin and Range Province, *J. Geophys. Res.*, *98*(B12), 22,109–22,122, doi:10.1029/93JB02641.

Zhu, L., and H. Kanamori (2000), Moho depth variation in southern California from teleseismic receiver functions, *J. Geophys. Res.*, *105*(B2), 2969–2980, doi:10.1029/1999JB900322.

J. S. Buehler and P. M. Shearer, Scripps Institution of Oceanography, University of California, San Diego, La Jolla, CA 92093-0225, USA. (jsbuehle@ucsd.edu)